Supporting Information

Bridging Lead Remediation and CO_2 Upgrading through Targeted Cation Exchange in an Ellagic Acid-based MOF

Song Chen, Junyao Chen, Ziyong Cheng, Jieying Hu, Hua-Qun Zhou, Lai-Hon Chung, Jun He**

School of Chemical Engineering and Light Industry, Guangdong University of Technology, Guangzhou, Guangdong 510006, P. R. China

Experimental details

Reagents and materials.

Ellagic acid (EA, 98%, isolated from chestnut bark) was purchased from MackLin. Lead(II) chloride ($PbCl_2$, 99%), lead(II) nitrate ($Pb(NO_3)_2$, 99%), lead(II) acetate trihydrate ($Pb(OAc)_2•3H_2O$), zinc nitrate ($Zn(NO_3)_2$, 99%), cadmium nitrate ($Cd(NO_3)_2$, 99%), cobalt(II) nitrate ($Co(NO_3)_2$, 99%), nickel(II) nitrate ($Ni(NO_3)_2$, 99%), *N*,*N*-dimethylformamide (DMF, 99.5%), *N*,*N*-dimethylacetamide (DMA, 99.5%), potassium bicarbonate ($KHCO_3$, AR), anhydrous ethanol (99.5%), dimethyl sulfoxide (DMSO, 99.8%), and deuterium oxide (D_2O, 99.9%) were purchased from Aladdin. 5 wt% Nafion solution and acetylene black were purchased from the Fuel Cell Store. All chemicals and materials were used without further purification.

Characterizations and instruments.

Powder X-ray diffraction (PXRD) spectra of the samples were recorded on a Rigaku SmartLab diffractometer (Japan) equipped with Cu *K*α radiation (λ = 1.54060 Å) at 40 kV and 200 mA. Fourier transform infrared (FT-IR) spectra were collected on a Thermo Scientific Nicolet Apex FTIR. X-ray photoelectron spectroscopy (XPS) measurements were carried out on a Thermo Scientific K-Alpha spectrometer using Al Kα radiation (hv = 1486.6eV). The working voltage is 12 kV, the filament current is 6 mA, and the charge correction is performed using C 1*s* = 284.80 eV as the energy standard. Scanning electron microscopy (SEM) images were acquired using a SU8010 microscope. Transmission electron microscopy (TEM) and high-resolution TEM (HR-TEM) images were collected on a JEOL JEM-F200 microscope operated at 120 kV. Cold field emission electron gun, rated power of 20 KW, equipped with JED-2300T EDS accessory from Japan Electronics, power consumption of 400W (detector type: 100 mm^2 SDD detector), energy resolution of 129 eV (Mn-Kα). After proper gradient dilution, the concentration of Pb^{2+} was measured by inductively coupled plasma mass spectrometer (ICP-MS) (Thermo Fisher, ICAP RQ). The Bruker AVANCE III 400 MHz Superconducting Fourier is used to collect NMR data. Formate was quantitatively analyzed using a DIONEX AQUION RFIC ion chromatograph with an AS11-HC anion-exchange column and 1 mM KOH as the eluent.

Preparation of SU-102.

The synthesis of **SU-102** was based on the reported method with some modifications.[1] EA (360 mg) and $ZrOCl_2•8H_2O$ (192 mg) were dissolved in a mixture of DMF (12 mL), CH_3COOH

(9 mL), and ultrapure H_2O (6 mL) in an eggplant flask. The mixture was refluxed at 90 ℃ for three days under stirring. After cooling to room temperature, the resulting suspension was centrifuged at 8,000 rpm for 10 minutes to collect the yellow precipitate. The solid was washed three times with ethanol and water and then dried overnight in an oven at 70 °C to afford the **SU-102** samples.

Preparation of SU-102-Pb.

In a typical synthesis, **SU-102** (20 mg) and 10 mg $Pb(NO_3)_2$ were placed in a 25-mL eggplant flask, followed by the addition of 3 mL of Ar-saturated ultrapure H_2O and 5 mL DMA. The mixture was ultrasonicated for 5 minutes. Then, the mixture was degassed by N_2 bubbling for 5 minutes and sealed. The reaction mixture was subsequently heated to 70 °C with vigorous stirring for 4 hours. After cooling to room temperature, the yellow precipitate was collected by centrifugation (10,000 rpm), washed five times with ultrapure H_2O and ethanol, and dried under vacuum at room temperature to yield **SU-102-Pb**. The method for synthesizing **SU-102-Pb** using lead salts with different anions is the same, except that $Pb(NO_3)_2$ is replaced with an equimolar amount of $PbCl_2$ or $Pb(OAc)_2•3H_2O$.

Larger batches of **SU-102-Pb** were synthesized using 1.2 g of **SU-102** and 0.4 g $Pb(NO_3)_2$ (3 mmol), which were added to an eggplant flask containing 100 mL of DMA and 60 mL of water. The reaction mixture was subsequently heated to 70 °C with vigorous stirring for 6 hours. After cooling to room temperature, the yellow precipitate was collected by centrifugation (10,000 rpm), washed 5 times with ultrapure H_2O and ethanol, and dried under vacuum at room temperature to yield **SU-102-Pb** (large scale).

Synthesis of SU-102-Pb from simulated lead-acid battery wastewater.

The industrial wastewater from lead-acid battery factories is often acidic, high-concentration, lead-containing wastewater with typical characteristics such as suspended solids, chemical oxygen demand, and turbulence.[2] Therefore, we used natural lake water as the primary water source (Figure S3) and filtered it only through a 0.22-micron membrane to remove common insoluble substances. Then, ions commonly found in industrial wastewater from lead-acid battery factories (Pb^{2+}, Cd^{2+}, Zn^{2+}, Co^{2+}, Ni^{2+}) were added and adjusted to acidic pH using HCl (Table S2). Then, **SU-102** (20 mg) was placed in a 25 mL eggplant flask, followed by the addition of 3 mL of simulated wastewater and 5 mL DMA. The mixture was ultrasonicated for 5 minutes. Then, the mixture was degassed by N_2 bubbling for 5 minutes and sealed. The reaction mixture was subsequently heated to 70 °C with vigorous stirring for 4

hours. After cooling to room temperature, the yellow precipitate was collected by centrifugation (10,000 rpm), washed five times with ultrapure H_2O and ethanol, and dried under vacuum at room temperature to yield **SU-102-Pb** (named industrial wastewater).

The preparation of the working electrode.

To improve the catalyst's dispersibility and the electrode's conductivity, 10 mg of ground samples and 10 mg of acetylene black (AB) were ground together. Then the mixture was added to a 1 mL solution [ethanol (500 μL), H_2O (400 μL), and Nafion solution (5 wt%, 100 μL)] to produce a black suspension. After 30 minutes of sonication, a uniformly mixed 50 μL suspension was directly spray-coated onto hydrophobic carbon paper (1 × 2 cm^2) to form a 1 × 1 cm^2 catalyst area with a catalyst loading density of ~0.5 mg cm^{-2}.

Electrochemical measurements.

All electrochemical measurements were carried out in a three-electrode system using a sealed, two-compartment H-type cell separated by a Nafion-117 proton-exchange membrane. Each compartment was filled with 40 mL $KHCO_3$ solution (0.5 M). A saturated Ag/AgCl and a carbon rod were used as the reference and counter electrodes, respectively. In this work, all the potentials were converted to the reversible hydrogen electrode (RHE) using the formula $E_{RHE} = E_{Ag/AgCl} + E^{\theta}_{Ag/AgCl} + 0.0592 \times pH$. Electrochemical measurements were performed using a CHI660E workstation. Before electrochemical measurement, the electrolyte was completely degassed by purging with high-purity Ar or CO_2 at a flow rate of 20 mL min^{-1} for 30 minutes, and linear sweep voltammetry (LSV) was performed at a scanning rate of 5 mV s^{-1}. Chronoamperometry (CA) was measured at fixed potentials to evaluate the performance of CO_2RR. The faradaic efficiencies (FEs) of products were calculated according to the following equation: $FE_{products} = (N \times F \times n_{products})/Q \times 100\%$, N is the number of electrons transferred for products (N = 2 for CO_2-to-CO/HCOOH conversion and H_2O-to-H_2 conversion), F is the Faraday constant (96485 C mol^{-1}), $n_{products}$ is the moles of products (mol) and Q is the total charge obtained from chronoamperometry (C).

The gaseous reduction products of CO_2RR were monitored by a gas chromatograph (Fuli GC9790Plus, argon as a carrier gas) equipped with a flame ionization detector (FID for CO detection) and a thermal conductivity detector (TCD for H_2 detection). The electrolyte solution was collected from the cathode chamber after electrolysis and characterized by ^{1}H NMR, with the electrolyte (0.45 mL) mixed with D_2O (0.15 mL) and DMSO-d_6 (2 mM, 0.02 mL). In addition, quantitative analysis of the electrolyte solution collected from the cathode chamber was performed using the NMR internal-standard method and ion chromatography.

***In situ* FT-IR study.**

The *in situ* FT-IR study was carried out on a Thermo Scientific Nicolet Apex spectrometer equipped with an MCT detector cooled with liquid N_2. The Pt-coated Si hemispherical prism (20 mm in diameter, MTI Corporation) was used as the conductive substrate for the catalyst and the IR reflection element. The catalyst suspensions were dropped on the Pt/Si surface as the working electrode. An Ag/AgCl electrode and a Pt wire were used as the reference and counter electrodes, respectively. A CO_2-saturated 0.5 M $KHCO_3$ solution was used as an electrolyte for the CO_2 reduction reaction.

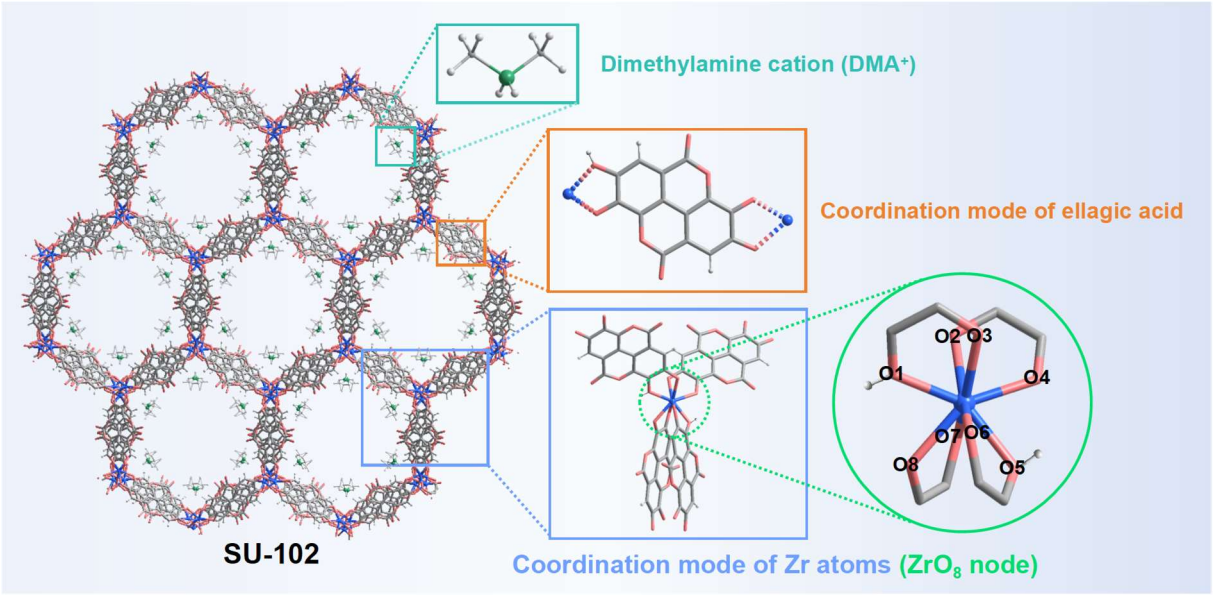

Fig. S1. Schematic diagram of the **SU-102** structure: ligand coordination mode, Zr atom coordination mode, and counter cation.

Fig. S2. Optical photos of gram-scale synthesis of **SU-102-Pb**.

Fig. S3. Optical photos of natural lake water (the top left picture shows the sample).

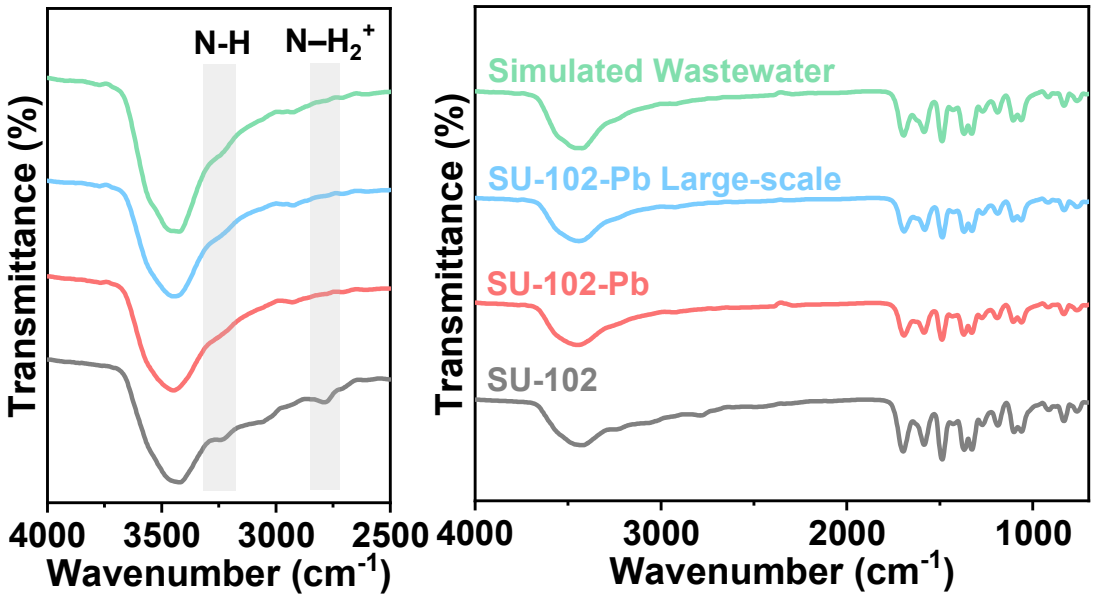

Fig. S4. FT-IR spectra of **SU-102** and **SU-102-Pb**.

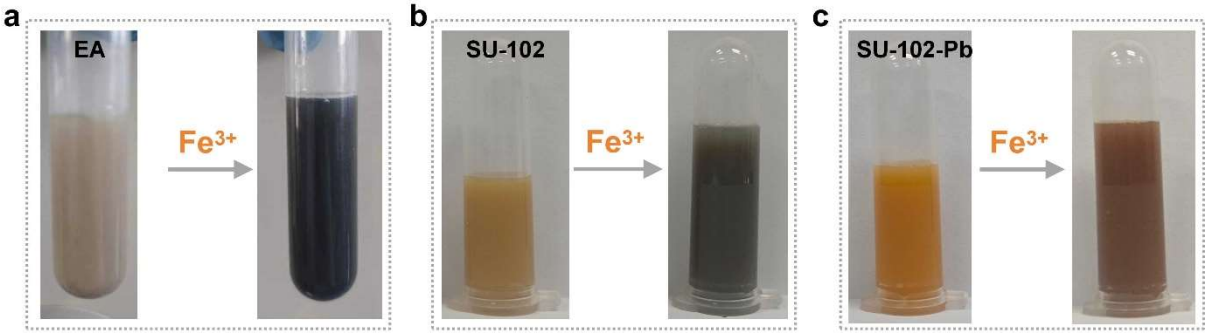

Fig. S5. Optical photos of color changes before and after introducing Fe^{3+} into EA, **SU-102**, and **SU-102-Pb** suspensions, respectively.

Note: It is reported that hydroxyl groups strongly chelate Fe^{3+}, combine quickly, and form a black product.[3] As shown in Figure S5a, the reaction between EA and Fe^{3+} rapidly produces black products. In Figure S5b, the reaction between **SU-102** and Fe^{3+} also produces a black product quickly, but the color is lighter than EA because only a small amount of –OH remains in **SU-102**.[1] In Figure S5c, the reaction between **SU-102-Pb** and Fe^{3+} also deepens the sample color, which indicates that there is still –OH in the MOF, but the color is even lighter because Pb has previously combined with –OH, which forms steric hindrance around –OH, hindering the reaction between Fe^{3+} and –OH.

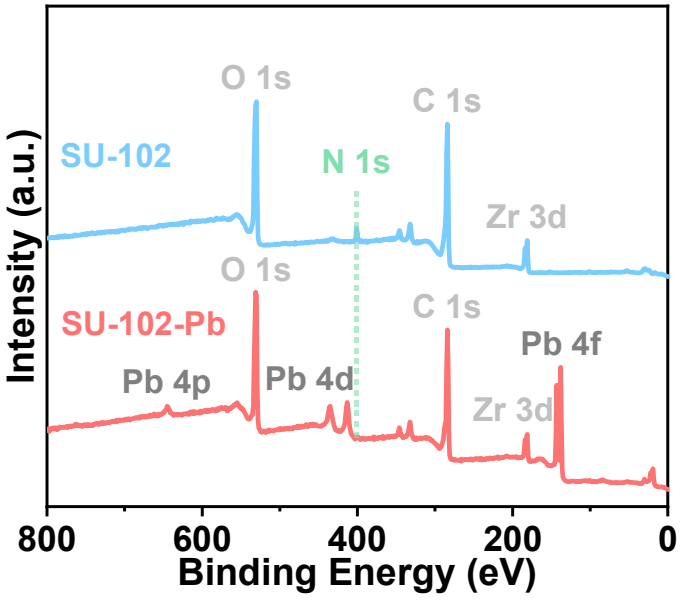

Fig. S6. XPS Survey spectra of **SU-102** and **SU-102-Pb**.

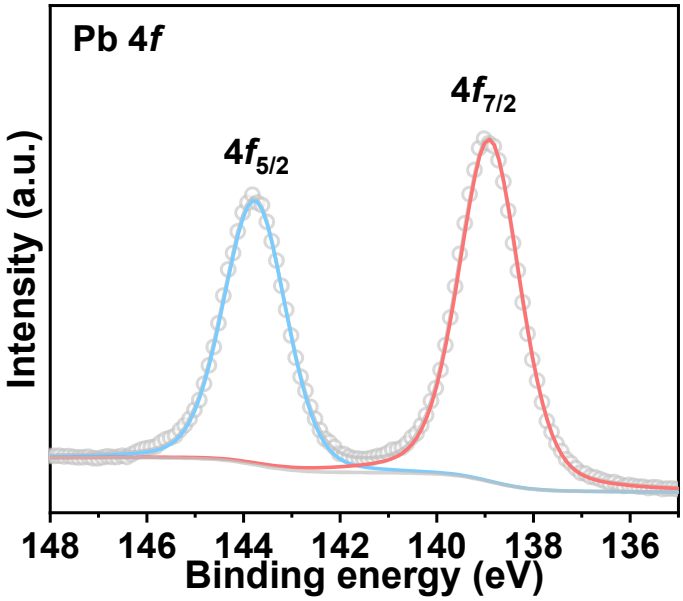

Fig. S7. XPS Pb 4*f* spectrum of **SU-102-Pb**.

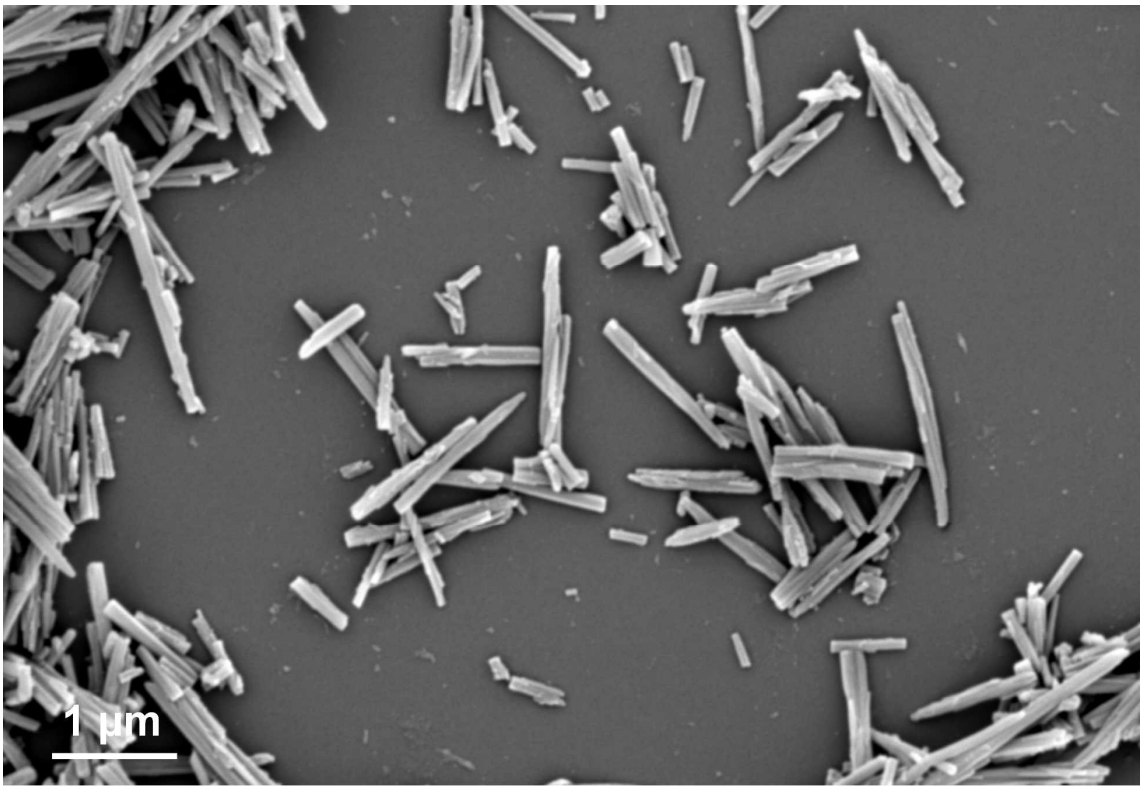

Fig. S8. SEM image of **SU-102**.

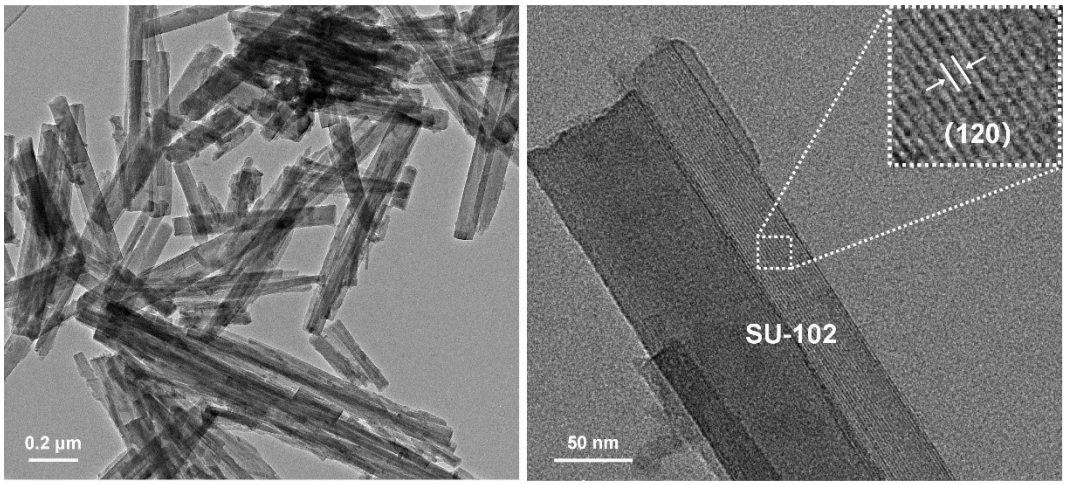

Fig. S9. TEM images of **SU-102** (inset showing lattice fringe of **SU-102**).

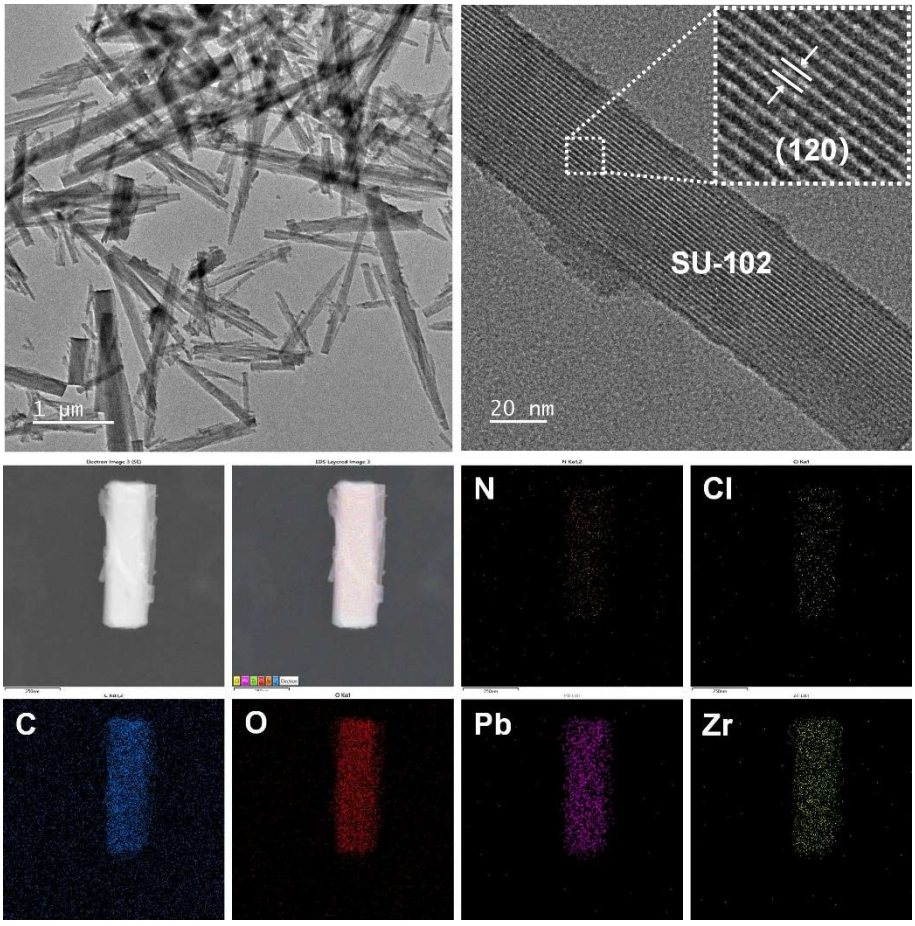

Fig. S10. TEM image of **SU-102-Pb** (inset showing lattice fringe of **SU-102-Pb**) and the corresponding elemental mapping of C, N, O, Cl, Zr and Pb.

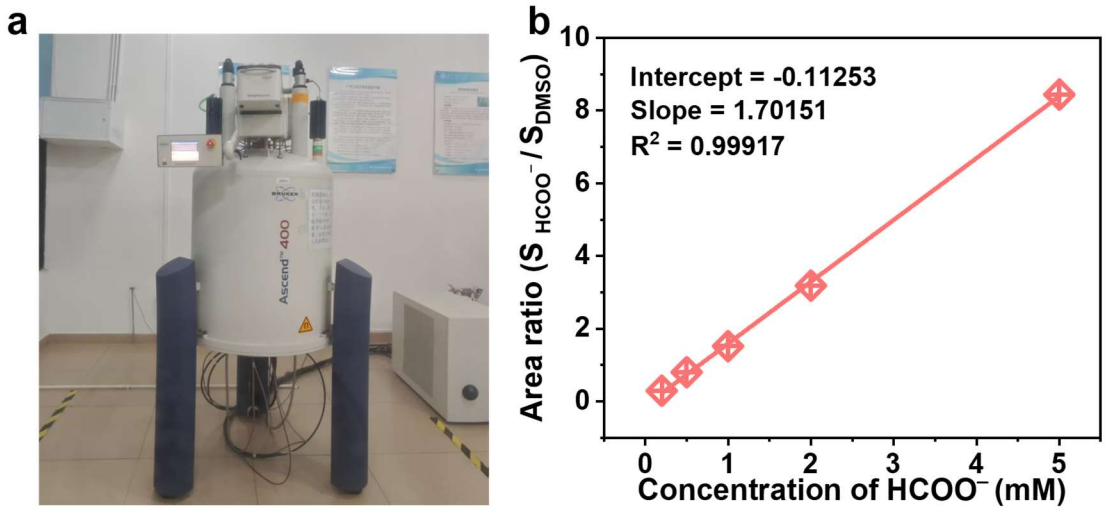

Fig. S11. (a) Bruker AVANCE III 400 MHz Nuclear Magnetic Resonance Spectrometer. (b) Standard curve of CO_2RR product ($HCOO^-$).

Fig. S12. Optical photograph of gas chromatography.

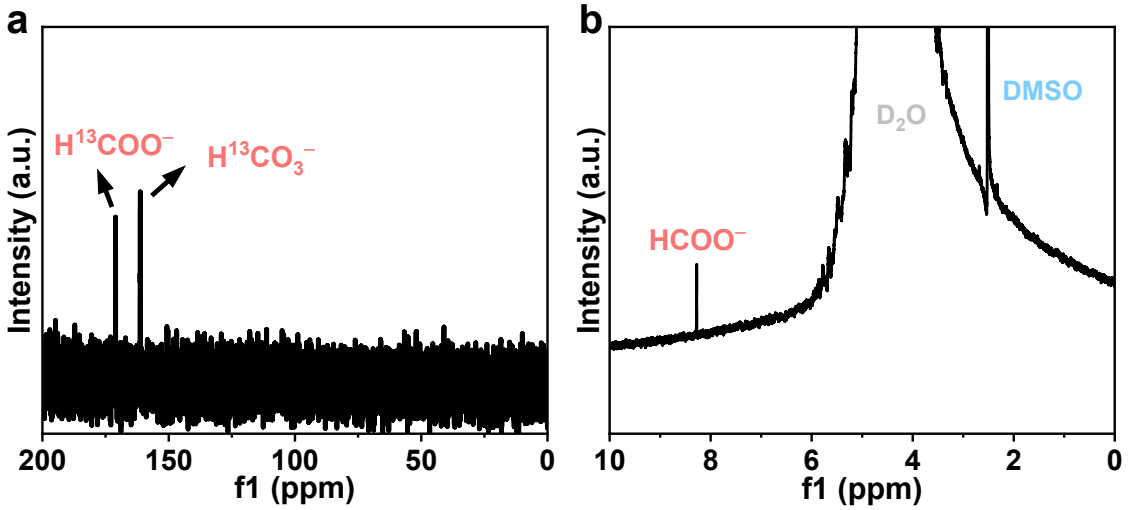

Fig. S13. ^{1}H NMR and ^{13}C NMR of eCO_2RR products from **SU-102-Pb**.

Note: The $H^{13}COO^-$ signal arises from the natural abundance of ^{13}C (^{12}C: 98.9%, ^{13}C: 1.1%). Although there is significant interference, the presence of this signal still proves that the electrolytic product is only $HCOO^-$.

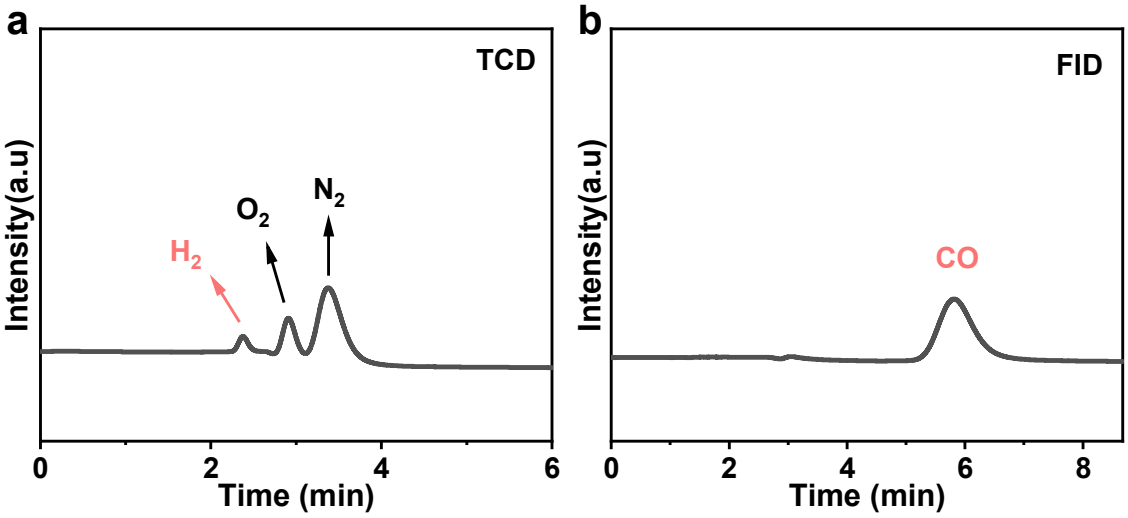

Fig. S14. Gas chromatograms of gas products collected after electrolysis.

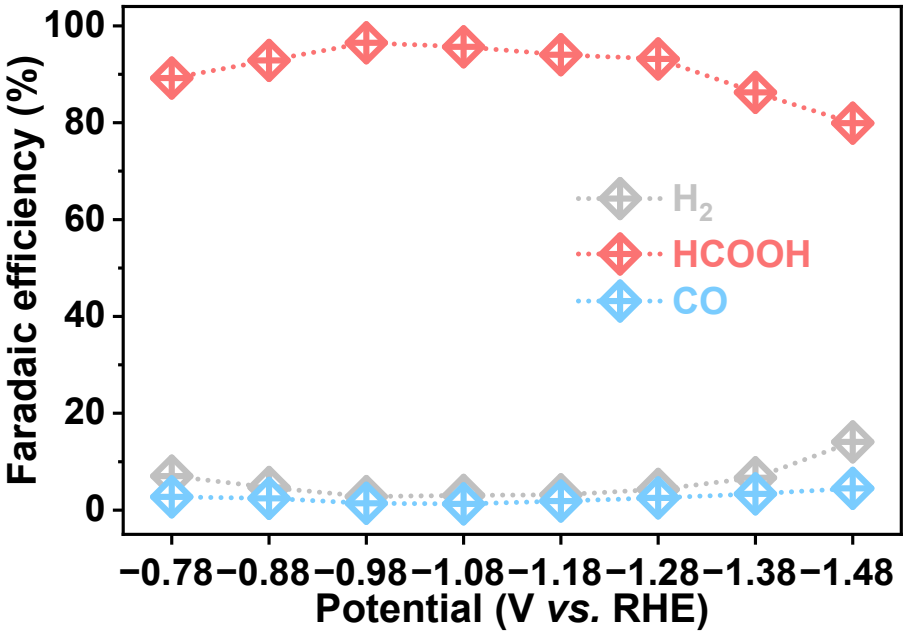

Fig. S15. *FE*s corresponding to $HCOO^-$, CO and H_2 of **SU-102-Pb** at different potentials.

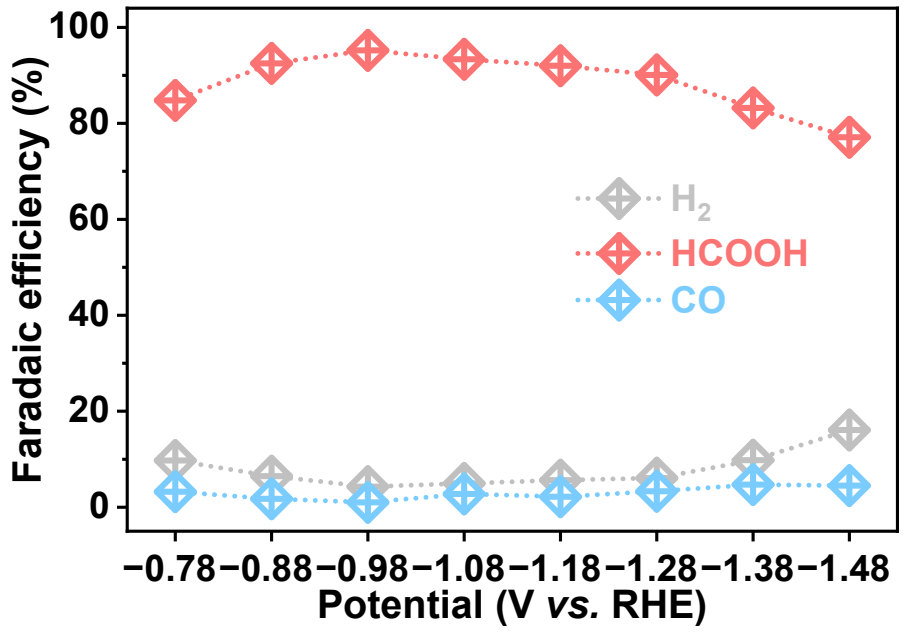

Fig. S16. *FE*s corresponding to $HCOO^-$, CO and H_2 of **SU-102-Pb** (large scale) at different potentials.

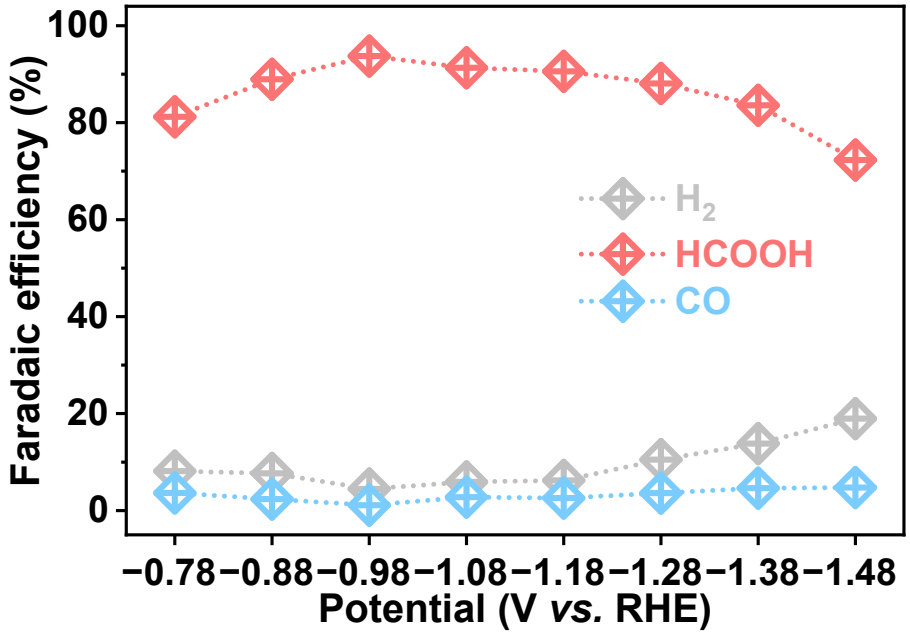

Fig. S17. *FE*s corresponding to $HCOO^-$, CO and H_2 of **SU-102-Pb** (industrial wastewater) at different potentials.

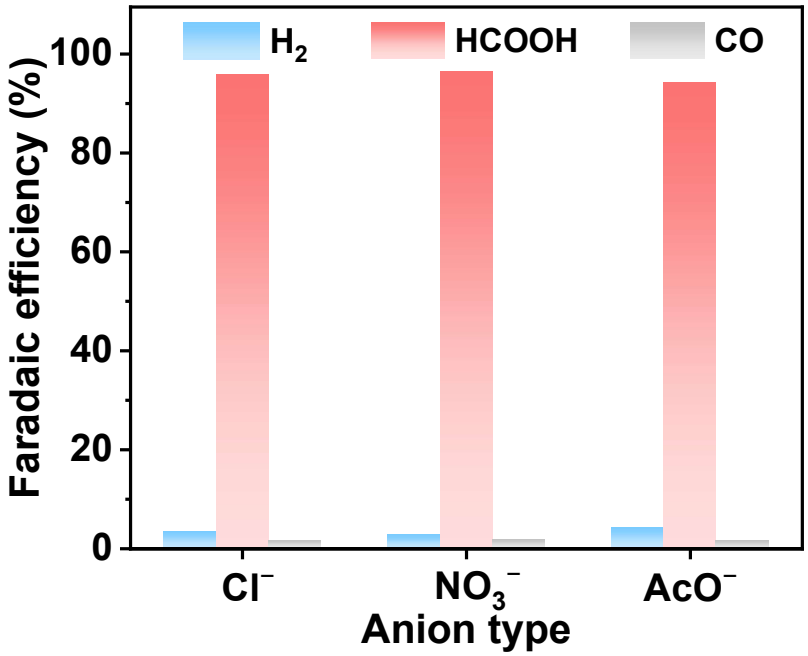

Fig. S18. *FE*s of CO_2RR at optimal voltage for **SU-102-Pb** catalysts synthesized using different Pb salts.

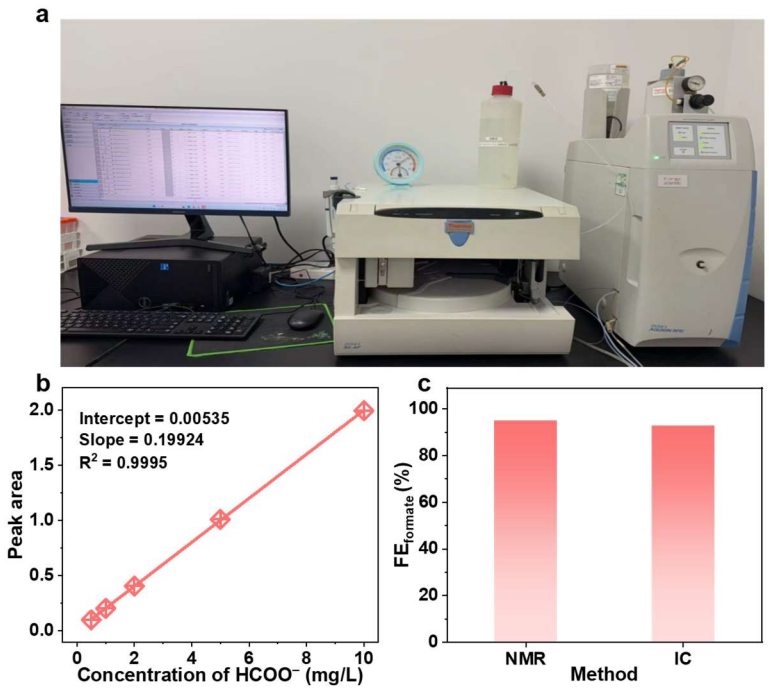

Fig. S19. (a) Optical photos of DIONEX AQUION RFIC ion chromatography. (b) Standard curve of CO_2RR product ($HCOO^-$). (c) The *FE*s of $HCOO^-$ were quantified by NMR and IC methods, respectively.

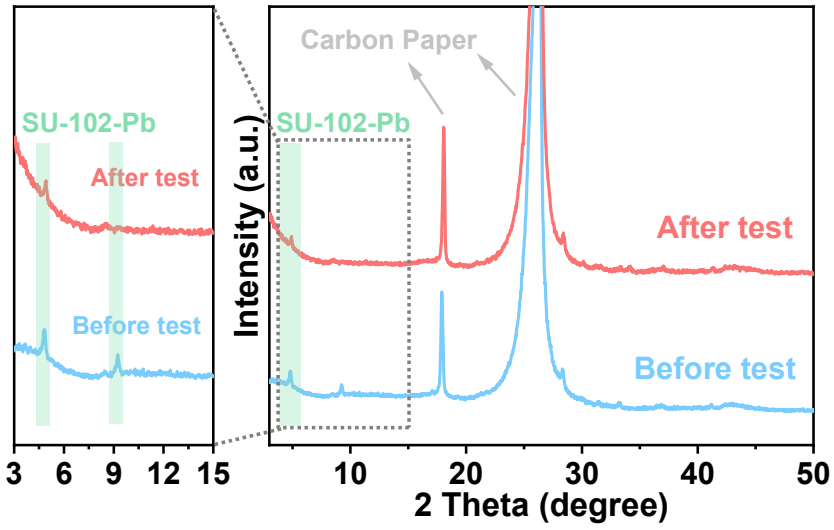

Fig. S20. PXRD patterns of **SU-102-Pb** before and after electrolysis. The weak diffraction peaks of **SU-102-Pb** arise largely from the low sample loading (0.5 mg MOF distributed on 1 cm^2 carbon paper).

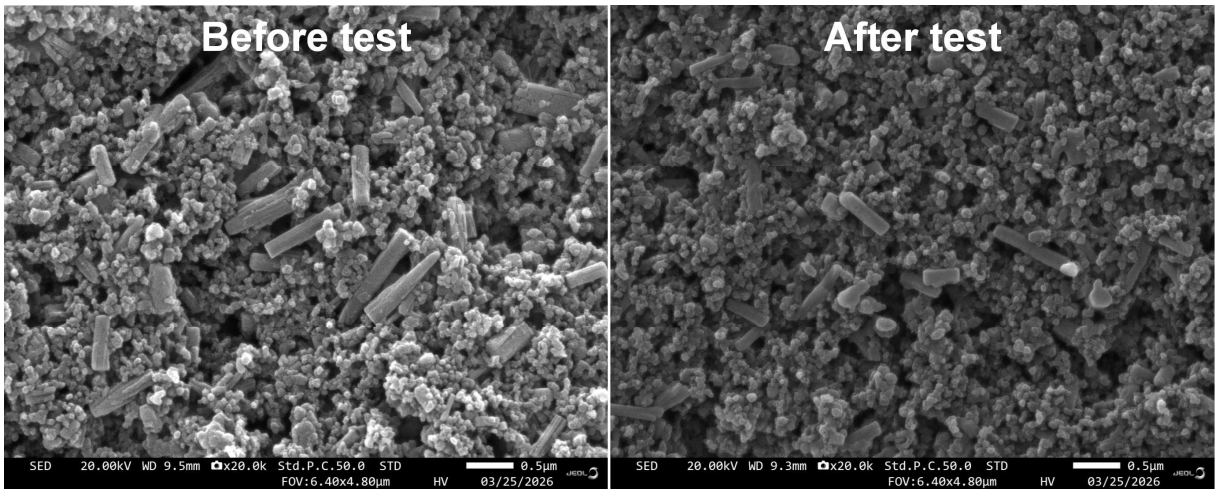

Fig. S21. SEM images of **SU-102-Pb** before and after long-term catalysis.

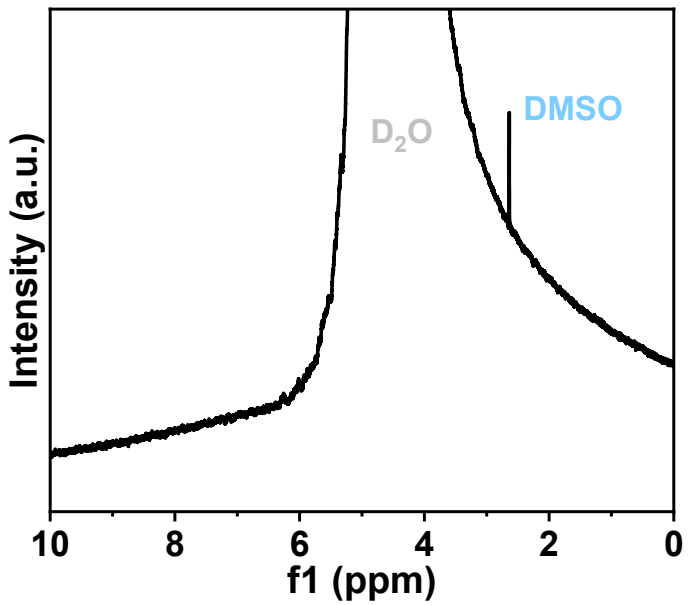

Fig. S22. ^{1}H NMR spectra of the electrolyte after electrolysis without a catalyst.

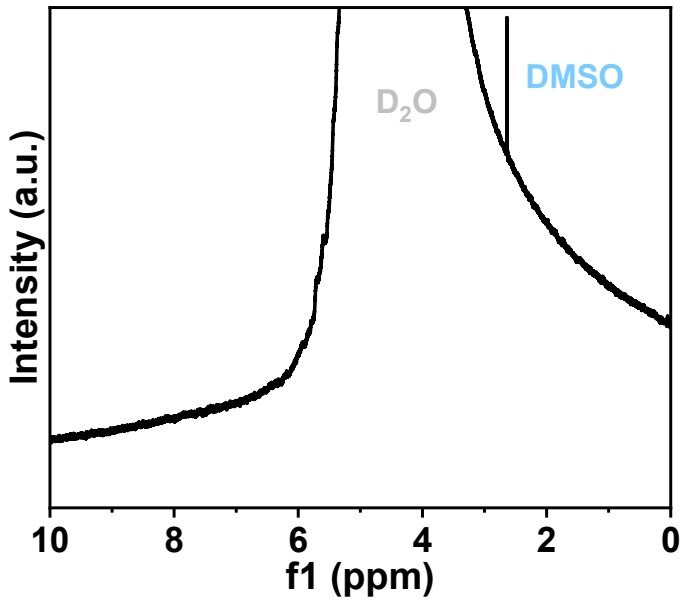

Fig. S23. ^{1}H NMR spectrum of electrolyte after electrolysis without CO_2.

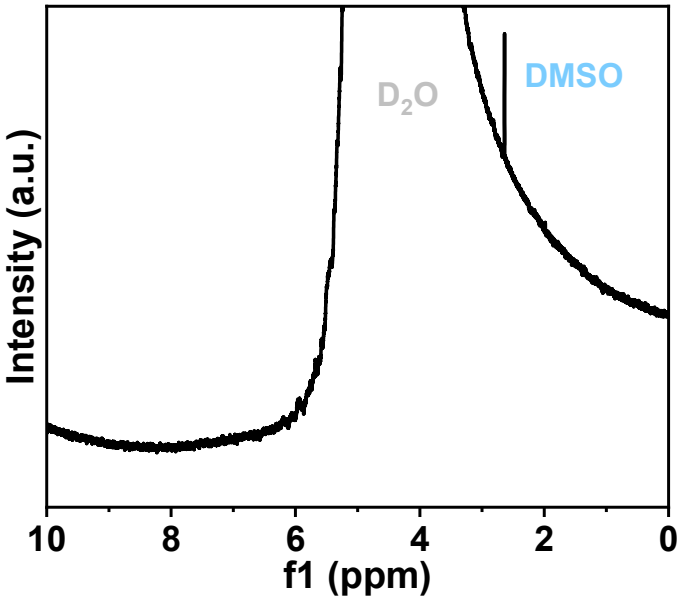

Fig. S24. ^{1}H NMR spectrum of eCO_2RR products from **SU-102**.

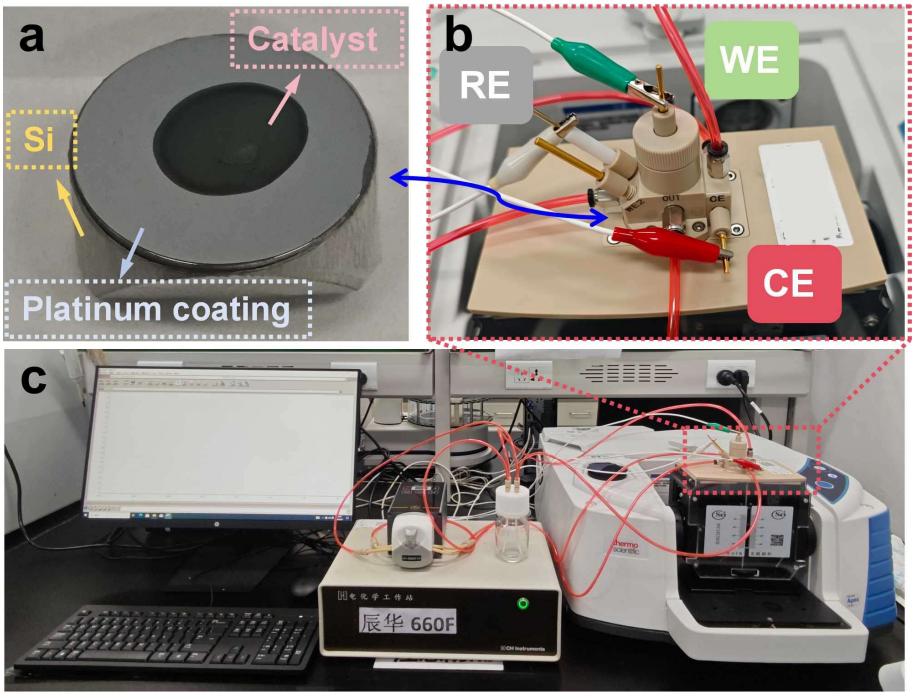

Fig. S25. The labeled photos of the experimental setup for *in situ* DRIFTS measurement: (a) Monocrystalline silicon, surface platinum layer, and sample coating. (b) Customized *in situ* infrared spectroscopy electrolytic cell. (c) Photo of an *in situ* testing device.

Table S1. Changes of Pb^{2+} concentration and removal rate after **SU-102-Pb** synthesis under different feed ratios and conditions.

Pb^{2+}concentrations (ppm)	Water source status	Pb^{2+} removal rate (%)
36	pure water pH = 7	98.87
36	industrial wastewater pH = 3.3	98.14
360	pure water pH = 7	98.84
360	industrial wastewater pH = 3.3	98.46
694	pure water pH = 7	98.64
694	industrial wastewater pH = 3.3	98.29

Table S2. Simulated lead-acid battery wastewater quality parameter table.

Parameters	**Unit**	**Value**
pH	/	3.3
Suspended solids (SS)	mg/L	16
Chemical oxygen demand (COD)	mg/L	24.7
Conductivity	mS/cm	13.45
Turbidity	NTU	0.3
TOC	mg/L	8.68
Pb^{2+}	mg/L	694.53
Zn^{2+}	mg/L	60.38
Cd^{2+}	mg/L	42.64
Ni^{2+}	mg/L	17.3
Co^{2+}	mg/L	20.54

Table S3. Elemental analysis and comparison of **SU-102** before and after Pb^{2+} incorporation.

Sample	N (%)	C (%)	H (%)	S (%)
SU-102	2.27	40.40	3.86	0.00
SU-102-Pb	0.00	27.50	2.55	0.00

Table S4. Pb content of **SU-102-Pb** determined by ICP-OES analysis.

Catalyst	Pb (wt%)
SU-102-Pb	19.68
SU-102-Pb (large scale)	17.84
SU-102-Pb (industrial wastewater)	16.98
SU-102-$PbCl_2$	19.16
SU-102-$Pb(OAc)_2$	18.49

Table S5. ICP analysis of various metal ion contents in **SU-102-Pb** (industrial wastewater) samples.

Sample	Pb (wt%)	Cd (wt%)	Co (wt%)	Ni (wt%)	Zn (wt%)
SU-102-Pb	16.98	0.0511	0.0396	0.0414	0.0627

Table S6. The content of Zr ions in the supernatant of **SU-102-Pb** synthesis.

Test element	Concentration (ppb)
Zr	0.2031

Table S7. The content of Pb ions in the electrolyte after long-term electrolysis

Sample	Test time (h)	Test element	Concentration (ppb)
SU-102-Pb	6	Pb	135.6

Table S8. Comparison of the performance of **SU-102-Pb** and reported Pb-based catalysts in H-type electrolytic cells under neutral conditions.

Catalysts	Electrolyte	Electrolysis potential (V *vs.* RHE)	Partial current density (mA cm^{-2})	FE (%)	Window (mV)	Reference
Zn(Pb)	0.1M $KHCO_3$	–1.2	–47	95	200	4
Pb dendrites	1 M $KHCO_3$	–0.99	–7.5	97	300	5
Nanolayered Pb	0.1 M $KHCO_3$	–1.1	N/A	94	400	6
Oxide-derived Pb	0.5 M $NaHCO_3$	–0.8	–0.6	98	300	7
Amine-modified Pb	1 M $KHCO_3$	–1.29	–24	80	200	8
Oxide-derived Sn-Pb-Sb	0.1 M $KHCO_3$	–1.4	–8.3	91	200	9
Sulfide-derived Pb	0.1 M $KHCO_3$	–1.08	–12	88	100	10
TA-Pb	0.5 M $NaHCO_3$	–0.92	–0.4	96.4	300	11
Roughened Pb	0.1M $KHCO_3$	–0.96	–1.2	88	100	12
$[Pb_3(CO_3)_2(OH)_2]$	0.1 M $KHCO_3$	–0.98	–7.3	96.8	200	13
PbNP/MWCNT/CPE	0.5 M $KHCO_3$	–1.03	–28	84.6	100	14
Pb-PhyA	Ionic Liquid	–1.58	–30	92.7	400	15
Co-$PbCO_3$	0.1 M $KHCO_3$	–0.7	–21.52	98.15	200	16
Pb_7Sn_1	0.5 M $KHCO_3$	–1.23	–11	90.53	200	17
Pb_7In_3	0.5 M $KHCO_3$	–1.26	–17	91.6	100	18
PbS	0.1 M $KHCO_3$	–1.2	–5.2	97.6	300	19
Pb(111)	0.1 M $KHCO_3$	–0.83	–2.4	98.3	400	20
EA-Pb	0.1 M $KHCO_3$	–1.08	–6.5	95.37	500	21
Porous Pb	0.5 M $KHCO_3$	–1.7 (*vs.* SCE)	–10	96.8	300	22
Pb_1Cu	0.5 M $KHCO_3$	–0.72	N/A	95.7	600	23
$PbSA_{100}$-Cu/Cp	0.5 M $KHCO_3$	–0.9	–27.9	97	300	24
Bi-Pb	0.5 M $KHCO_3$	–0.8	–53.1	97.8	400	25
$BiPbO_2Br$	0.5 M $KHCO_3$	–0.9	–40	96.6	400	26
SU-102-Pb	**0.5 M $KHCO_3$**	**–0.98**	**–17**	**96.5**	**600**	**This Work**

Reference

[1] E. S. Grape, A. J. Chacón-García, S. Rojas, Y. Pérez, A. Jaworski, M. Nero, M. Åhlén, E. Martínez-Ahumada, A. E. G. Feindt, M. Pepillo, M. Narongin-Fujikawa, I. A. Ibarra, O. Cheung, C. Baresel, T. Willhammar, P. Horcajada, A. K. Inge, *Nat. Water* **2023**, *1*, 433–442.

[2] Y. Wang, Y. Shang, Z. Fu, K. Li, J. Shi, L. Xu, P. Jin, X. Jin, X. C. Wang, *J. Hazard. Mater.* **2025**, *490*, 137670.

[3] a) S. Chen, Y. Qian, Z. Cheng, L.-H. Chung, W. Ou, J. Hu, Q. Mo, S. Chen, J. He, H.-L. Jiang, *Angew. Chem. Int. Ed*. **2026**, *65*, e8338805; b) G. Zhang, S. A. Amin, F. C. Küpper, P. D. Holt, C. J. Carrano, A. Butler, *Inorg. Chem.* **2009**, *48*, 11466–11473; c) N. von Wirén, H. Khodr, R. C. Hider, *Plant Physiol*. **2020**, *124*, 1149–1157.

[4] A. G. A. Mohamed, E. Zhou, Z. Zeng, J. Xie, D. Gao, Y. Wang, *Adv. Sci*. **2022**, *9*, 2104138.

[5] M. Fan, S. Garbarino, G. A. Botton, A. C. Tavares, D. Guay, *J. Mater. Chem. A* **2017**, *5*, 20747–20756.

[6] Y. Kwon, J. Lee, *Electrocatal*. **2010**, *1*, 108–115

[7] C. H. Lee, M. W. Kanan, *ACS Catal*. **2015**, *5*, 465–469.

[8] N. Zouaoui, B. D. Ossonon, M. Fan, D. Mayilukila, S. Garbarino, G. de Silveira, G. A. Botton, D. Guay, A. C. Tavares, *J. Mater. Chem. A* **2019**, *7*, 11272–11281.

[9] S. Rasul, A. Pugnant, H. Xiang, J.-M. Fontmorin, E. H. Yu, *J CO_2 Util*. **2019**, *32*, 1–10

[10] J. E. Pander, J. W. J. Lum, B. S. Yeo, *J. Mater. Chem. A* **2019**, *7*, 4093–4101.

[11] Y. Shi, Y. Ji, J. Long, Y. Liang, Y. Liu, Y. Yu, J. Xiao, B. Zhang, *Nat. Commun*. **2020**, *11*, 3415.

[12] Z. He, J. Shen, Z. Ni, J. Tang, S. Song, J. Chen, L. Zhao, *Catal. Commun*. **2015**, *72*, 38–42

[13] D. Wang, S. Dong, L. Wen, W. Yu, Z. He, Q. Guo, X. Lu, L. Wang, S. Song, J. Ma, *Chemosphere* **2022**, *291*, 132889.

[14] Y. Xing, M. Cui, P. Fan, J. Ren, C. Zhang, N. Li, X. Wen, X. Ji, *Mater. Chem. Phys*. **2019**, *237*, 121826.

[15] H. Wu, J. Song, C. Xie, Y. Hu, J. Ma, Q. Qian, B. Han, *Green Chem*. **2018**, *20*, 4602–4606.

[16] N. Zhang, D. Li, X. Wang, R. Cai, C.-L. Dong, T. Thi Thuy Nga, L. Zhang, D. Yang, *Appl. Catal. B* **2023**, *326*, 122404.

[17] Q. Wang, Y. Guan, J. Yan, Y. Liu, Q. Shao, F. Ning, J. Yi, *Dalton Trans*. **2023**, *52*, 4136–4141

[18] X. Sun, X. Shao, J. Yi, J. Zhang, Y. Liu, *Chemosphere* **2022**, *293*, 133595.

[19] Z. Zhang, C. Liu, J. T. Brosnahan, H. Zhou, W. Xu, S. Zhang, *J. Mater. Chem. A* **2019**, *7*, 23775–23780.

[20] W. Yu, L. Wen, J. Gao, S. Chen, Z. He, D. Wang, Y. Shen, S. Song, *Chem. Commun*. **2021**, *57*, 7418–7421.

[21] S. Chen, L.-H. Chung, S. Chen, Z. Jiang, N. Li, J. Hu, W.-M. Liao, J. He, *Small* **2024**, *20*, 2400978.

[22] J. Wang, H. Wang, Z. Han, J. Han, *Front. Chem. Sci. Eng*. **2015**, *9*, 57–63.

[23] T. Zheng, C. Liu, C. Guo, M. Zhang, X. Li, Q. Jiang, W. Xue, H. Li, A. Li, C.-W. Pao, J. Xiao, C. Xia, J. Zeng, *Nat. Nanotechnol*. **2021**, *16*, 1386.

[24] Y. Xu, X. Liu, M. Jiang, B. Chi, Y. Lu, J. Guo, Z. Wang, S. Cui, *J. Colloid Interf. Sci*. **2024**, *665*, 365–375.

[25] C. Jiang, S. Zeng, J. Feng, G. Li, B. Hai, K. Peng, X. Zhang, *J. Mater. Chem. A*, **2024**, *12*, 14809–14815.

[26] G. Sun, C. Zou, W. Sun, Y. Fang, S. He, Y. Liu, J. Zhang, Y. Zhu, J. Wang, *Mater. Chem. Front*. **2023**, *7*, 3382–3389.